Monthly Notices
of the
ROYAL ASTRONOMICAL SOCIETY

Mon. Not. R. Astron. Soc. **410,** 573–584 (2011) doi:10.1111/j.1365-2966.2010.17466.x

Luminosity functions of local infrared galaxies with *AKARI*: implications for the cosmic star formation history and AGN evolution

Tomotsugu Goto,[1,2⋆] Stephane Arnouts,[3] Hanae Inami,[4] Hideo Matsuhara,[5] Chris Pearson,[6,7,8] Tsutomu T. Takeuchi,[9] Emeric Le Floc'h,[10] Toshinobu Takagi,[5] Takehiko Wada,[5] Takao Nakagawa,[5] Shinki Oyabu,[11] Daisuke Ishihara,[9] Hyung Mok Lee,[12] Woong-Seob Jeong,[13] Chisato Yamauchi,[5] Stephen Serjeant,[8] Chris Sedgwick[8] and Ezequiel Treister[1]

[1]*Institute for Astronomy, University of Hawaii, 2680 Woodlawn Drive, Honolulu, HI 96822, USA*
[2]*Subaru Telescope, 650 North A'ohoku Place, Hilo, HI 96720, USA*
[3]*Canada–France–Hawaii Telescope, 65-1238 Mamalahoa Hwy, Kamuela, HI 96743, USA*
[4]*Spitzer Science Center, California Institute of Technology, Pasadena, CA 91125, USA*
[5]*Institute of Space and Astronautical Science, Japan Aerospace Exploration Agency, Sagamihara, Kanagawa 252–5210, Japan*
[6]*RAL Space, Rutherford Appleton Laboratory, Chilton, Didcot, Oxfordshire OX11 0QX*
[7]*Institute for Space Imaging Science, University of Lethbridge, Lethbridge, Alberta, T1K 3M4, Canada*
[8]*Astrophysics Group, The Department of Physics and Astronomy, The Open University, Milton Keynes MK7 6AA*
[9]*Institute for Advanced Research, Nagoya University, Furo-cho, Chikusa-ku, Nagoya 464-8601, Japan*
[10]*CEA-Saclay, Service d'Astrophysique, France*
[11]*Graduate School of Science, Nagoya University, Furo-cho, Chikusa-ku, Nagoya, Aichi 464-8602, Japan*
[12]*Department of Physics & Astronomy, FPRD, Seoul National University, Shillim-Dong, Kwanak-Gu, Seoul 151–742, Korea*
[13]*Korea Astronomy and Space Science Institute, 61-1, Hwaam-dong, Yuseong-gu, Daejeon 305–348, Korea*

Accepted 2010 July 30. Received 2010 July 26; in original form 2010 April 28

ABSTRACT

Infrared (IR) luminosity is fundamental to understanding the cosmic star formation history and active galactic nuclei (AGN) evolution, since their most intense stages are often obscured by dust. However, local IR luminosity function estimates today are still based on the *IRAS* survey in the 1980s, with wavelength coverage only up to 100 μm. The *AKARI* IR space telescope performed an all-sky survey in six IR bands (9, 18, 65, 90, 140 and 160 μm) with 3–10 times better sensitivity, covering the crucial far-IR wavelengths across the peak of the dust emission. Combined with a better spatial resolution, *AKARI* can much more precisely measure the total infrared luminosity ($L_{\rm TIR}$) of individual galaxies, and thus, the total infrared luminosity density in the local Universe.

By fitting modern IR spectral energy distribution (SED) models, we have remeasured $L_{\rm TIR}$ of the *IRAS* Revised Bright Galaxy Sample, which is a complete sample of local galaxies with $S_{60\,\mu{\rm m}} > 5.24$ Jy.

We present mid-IR monochromatic luminosity (νL_ν) to $L_{\rm TIR}$ correlations for *Spitzer* 8 μm, *AKARI* 9 μm, *IRAS* 12 μm, *WISE* 12 μm, *ISO* 15 μm, *AKARI* 18 μm, *WISE* 22 μm and *Spitzer* 24 μm filters. These measures of $L_{\rm MIR}$ are well correlated with $L_{\rm TIR}$, with scatter in the range 13–44 per cent. The best-fitting $L_{\rm MIR}$-to-$L_{\rm TIR}$ conversions provide us with estimates of $L_{\rm TIR}$ using only a single MIR band, in which several deep all-sky surveys are becoming available such as *AKARI* MIR and *WISE*.

Although we have found some overestimates of $L_{\rm TIR}$ by *IRAS* due to contaminating cirrus/sources, the resulting *AKARI* IR luminosity function (LF) agrees well with that from *IRAS*. We integrate the LF weighted by $L_{\rm TIR}$ to obtain a cosmic IR luminosity density of $\Omega_{\rm TIR} = (8.5^{+1.5}_{-2.3}) \times 10^7\,{\rm L}_\odot\,{\rm Mpc}^{-3}$, of which 7 ± 1 per cent is produced by luminous infrared

⋆E-mail: tomo@ifa.hawaii.edu

galaxies (LIRGs) ($L_{\rm TIR} > 10^{11}\,{\rm L}_{\odot}$), and only 0.4 ± 0.1 per cent is from ultraluminous infrared galaxies (ULIRGs) ($L_{\rm TIR} > 10^{12}\,{\rm L}_{\odot}$) in the local Universe, in stark contrast to high-redshift results.

We separate the contributions from AGN and star-forming galaxies (SFGs). The SFG IR LF shows a steep decline at the bright end. Combined with high-redshift results from the *AKARI* NEP deep survey, these data show a strong evolution of $\Omega_{\rm TIR}^{\rm SF} \propto (1+z)^{4.0\pm0.5}$ and $\Omega_{\rm TIR}^{\rm AGN} \propto (1+z)^{4.4\pm0.4}$. For $\Omega_{\rm TIR}^{\rm AGN}$, the ULIRG contribution exceeds that from LIRGs already by $z \sim 1$. A rapid evolution in both $\Omega_{\rm TIR}^{\rm AGN}$ and $\Omega_{\rm TIR}^{\rm SFG}$ suggests the correlation between star formation and black hole accretion rate continues up to higher redshifts. We compare the evolution of $\Omega_{\rm TIR}^{\rm AGN}$ to that of X-ray luminosity density. The $\Omega_{\rm TIR}^{\rm AGN} / \Omega_{\rm X-ray}^{\rm AGN}$ ratio shows a possible increase at $z > 1$, suggesting an increase of obscured AGN at $z > 1$.

Key words: galaxies: evolution – galaxies: formation – galaxies: interactions – galaxies: peculiar – galaxies: starburst – infrared: galaxies.

1 INTRODUCTION

To understand the cosmic history of star formation and black hole growth, we must understand infrared (IR) emission; the more intense the star formation, the more deeply it is embedded in the dust, hence, such star formation is not visible in the ultraviolet (UV) but in the infrared. Similarly, active galactic nuclei (AGN) evolutionary scenarios predict that they are heavily obscured at their youngest, Compton-thick stage (Treister, Urry & Virani 2009). The *Spitzer* and *AKARI* satellites revealed large amounts of infrared emission in the high-redshift Universe, showing strong evolution in the infrared luminosity density (Le Floc'h et al. 2005; Pérez-González et al. 2005; Babbedge et al. 2006; Caputi et al. 2007; Magnelli et al. 2009). For example, at $z = 1$, Goto et al. (2010) estimated 90 per cent of star formation activity is hidden by dust. However, the key baseline of these evolution studies is still at $z = 0$, using a local infrared LF from the *IRAS* survey in the 1980s.

For more than 25 years, bolometric infrared luminosities ($L_{\rm TIR,8-1000\,\mu m}$) of local galaxies have been estimated using a simple polynomial presented by Pérault (1987), obtained assuming a simple blackbody and dust emissivity. Furthermore, the reddest filter of *IRAS* is 100 μm, which does not span the peak of the dust emission for most galaxies, leaving a great deal of uncertainty. A number of studies found cold dust that cannot be detected with *IRAS*. For example, Dunne & Eales (2001) detected such cold dust with $T \sim 20$ K using SCUBA 450- and 850-μm observations. Symeonidis et al. (2009) detected cold galaxies with spectral energy distribution (SED) peaks at longer wavelengths using *Spitzer*/MIPS. These results cast further doubt on $L_{\rm TIR}$ estimation made with only <100-μm photometry. More precise estimates of the local $L_{\rm TIR}$ and thus the local IR luminosity function (LF) have been long awaited, to be better compared with high-redshift work.

AKARI, the Japanese infrared satellite (Murakami et al. 2007), provides the first chance to rectify the situation since *IRAS*; *AKARI* performed an all-sky survey in two mid-infrared (centred on 9 and 18 μm) and four far-infrared bands (65, 90, 140 and 160 μm). Its 140 and 160 μm are especially important to cover across the peak of the dust emission, allowing us to accurately measure the Rayleigh–Jeans tail of the IR emission. The time is ripe in terms of modelling as well: several sophisticated infrared SED models have become available (Chary & Elbaz 2001; Dale & Helou 2002; Lagache, Dole & Puget 2003; Siebenmorgen & Krügel 2007), from which we can not only obtain accurate $L_{\rm TIR}$ estimates, but also constrain the astrophysics.

In this work, we aim to remeasure the local $L_{\rm TIR}$, and thereby the IR LF of the Revised Bright Galaxy Sample (RBGS, Sanders et al. 2003), which is a complete sample of local IR galaxies. This work provides us with an important local benchmark on which to base future evolution studies at high redshift both by the current *AKARI* and *Spitzer* satellites, and by next-generation IR satellites such as *Herschel*, *WISE*, *JWST* and *SPICA*. We adopt a cosmology with $(h, \Omega_{\rm m}, \Omega_{\Lambda}) = (0.75, 0.3, 0.7)$ for a comparison.

2 THE *AKARI* ALL-SKY SURVEY AND RBGS

In this work, we use the $\beta 1$ version of the *AKARI*/IRC bright source catalogue and the $\beta 2$ version of the *AKARI*/FIS bright source catalogue. The 5σ sensitivities in the *AKARI* IR filters (S9W, L18W, N60, WS, WL and N160) are 0.05, 0.09, 2.4, 0.55, 1.4 and 6.3 Jy (Yamamura et al. 2009; Ishihara et al. 2010). In addition to the much improved sensitivity and spatial resolution over its precursor (*IRAS*), the presence of 140- and 160-μm bands is crucial to measure the peak of the dust emission at FIR wavelengths, and thus the $L_{\rm TIR}$ of galaxies, especially the ones with lower dust temperature.

We have cross-correlated the *AKARI* bright source catalogue with the Revised Bright Galaxy Sample (RBGS; Sanders et al. 2003), using a matching radius of 60 arcsec, as shown in Fig. 1. The RBGS is a complete, flux-limited survey of all extragalactic objects with 60-μm flux density greater than 5.24 Jy, covering the entire sky at $|b| > 5^{\circ}$. All the 629 objects in this catalogue have measured spectroscopic redshifts from either optical or millimetre/radio (CO or H I data). The maximum redshift of our sample is 0.087. Because of the completeness and availability of the spectroscopic redshifts, this catalogue is suitable to construct local infrared luminosity functions (LFs). In addition, each galaxy has a measured IR luminosity from the *IRAS* survey, allowing us to compare with the *AKARI*-based one. Due to the difference in sky coverage (*IRAS* covers 96 per cent of the sky, and *AKARI* covers 94 per cent), 24 galaxies out of 629 RBGS galaxies did not have an *AKARI* counterpart. We removed these galaxies from our analysis, but applied corresponding completeness corrections to our statistical analysis.

One important caveat is that the RBGS is a flux-limited sample from *IRAS* ($S_{60\,\mu m} > 5.24$ Jy). Therefore, if the *IRAS* $S_{60\,\mu m}$ flux was an overestimate as we will discuss later in the paper, our work does not address incompleteness in the sample selection. However, at this very low redshift (average redshift of 0.0082), the RBGS is still the largest complete sample of IR galaxies with spectroscopic redshift.

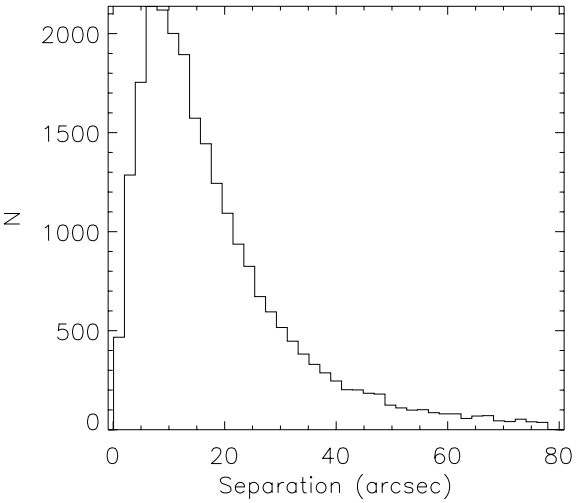

Figure 1. Angular separation between *AKARI* FIS and *IRAS* sources. We matched sources within 60 arcsec of separation.

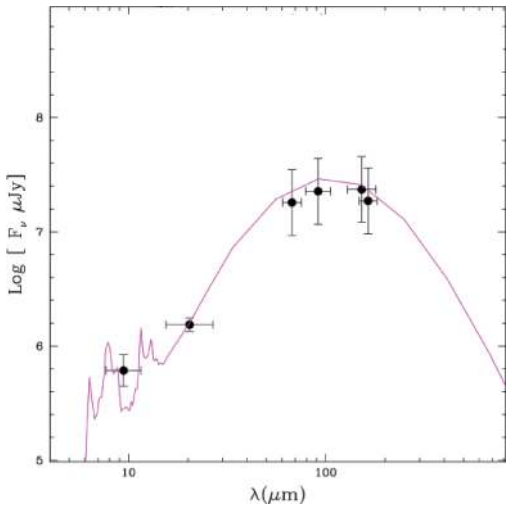

Figure 2. An example of the SED fit. We fit the *AKARI* six-band photometry to the SED model of Chary & Elbaz (2001) to estimate $L_{\rm TIR}$.

3 INFRARED LUMINOSITY

3.1 Estimating total IR luminosity

For these galaxies, we estimated new total IR luminosities ($L_{\rm TIR}$) based on the *AKARI* photometry using the LePhare code[1] to fit the infrared part (>7 μm) of the SED and estimate TIR luminosity. We fit our *AKARI* FIR photometry with the SED templates from Chary & Elbaz (2001, hereafter CHEL). Although the shapes of these SEDs are luminosity dependent, the large baseline from *AKARI* observations (S9W, L18W, N60, WS, WL and N160) allows us to adopt a free scaling to get the best SED fit, which is then rescaled to derive $L_{\rm TIR}$. Since the *AKARI* catalogues are the β-version, we adopted a minimum error of 25 per cent. Fig. 2 shows an example of the SED fit. At the median redshift of 0.0082 of the RBGS, peculiar velocity is not negligible. Therefore, instead of the measured redshift, we used the distance, which is corrected for heliocentric redshift using the cosmic attractor model (Mould et al. 2000) for the SED fitting and to compute $L_{\rm TIR}$. In this work, $L_{\rm TIR}$ is measured in the wavelength range of 8–1000 μm.

[1] http://www.cfht.hawaii.edu/~arnouts/lephare.html

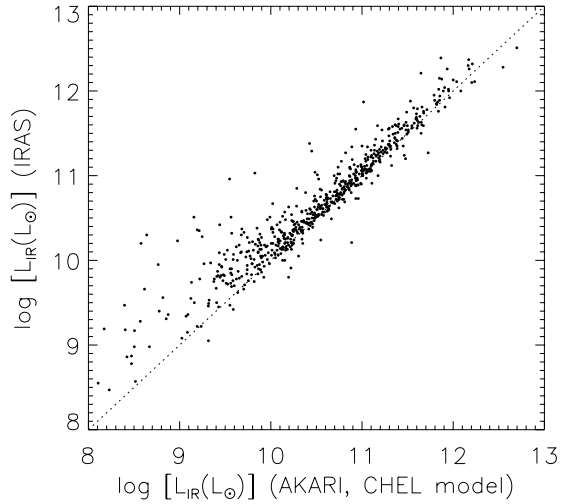

Figure 3. $L_{\rm TIR}$ measured by *AKARI* is compared with those measured by *IRAS* (equation 1) for the RBGS.

We chose not to use *IRAS* 12-, 25-, 60- and 100-μm fluxes in the SED fitting. Due to the detector pixel size, *AKARI* has significantly better spatial resolution (30–40 arcsec) than *IRAS* (1–2 arcmin). In a few per cent of cases, *AKARI* measured significantly lower flux than *IRAS*, because *AKARI* can subtract the background cirrus better, and/or can separate nearby confusing sources better [see Jeong et al. (2007) for more details].

In Fig. 3, we compare $L_{\rm TIR}$ measured by *AKARI* with those by *IRAS*. The *IRAS*-based $L_{\rm TIR}$ is measured using the following equation:

$$L_{\rm TIR}(\mathrm{L}_\odot) \equiv 4.93 \times 10^{-22}[13.48L_\nu(12\,\mu\mathrm{m}) + 5.16L_\nu(25\,\mu\mathrm{m}) + 2.58L_\nu(60\,\mu\mathrm{m}) + L_\nu(100\,\mu\mathrm{m})]\,\mathrm{erg\,s^{-1}\,Hz^{-1}}. \quad (1)$$

This equation is obtained by fitting a single-temperature dust emissivity model ($\epsilon \propto \nu^{-1}$) to the flux in all four *IRAS* bands and should be accurate to ±5 per cent for dust temperatures in the range of 25–65 K (Pérault 1987). The $L_{\rm TIR}$ measured by *AKARI* agrees well with those by *IRAS*. However, the scatter increases towards lower luminosity in $L_{\rm TIR}$ measured by *AKARI* than by *IRAS*, especially at $\log(L_{\rm TIR}) < 10$. This is primarily because *AKARI*'s higher spatial resolution can separate background cirrus or confusing sources better than *IRAS*, resulting in lower $L_{\rm TIR}$.

3.2 Model-to-model variation

In this section, we check the SED model dependence of $L_{\rm TIR}$ measurements. The IR SED models we used are Chary & Elbaz (2001), Dale & Helou (2002) and Lagache et al. (2003). We used these models to compute $L_{\rm TIR}$ exactly as described in Section 3.1. In Fig. 4, we plot the measured $L_{\rm TIR}$ against the model results, and find a tight correlation. As shown in Table 1, the standard deviations between different $L_{\rm TIR}$s are 10–24 per cent. The agreements are quite good considering the large flux errors (~25 per cent) associated with infrared photometry. Median offsets between them are $-13 \sim +24$ per cent, which could also be caused by calibration problems. In Table 1, the CHEL model shows the smallest offsets from other models. For k-correction and for $L_{\rm TIR}$ estimation (Section 3.1), we adopt CHEL models, which give luminosities in between the Dale models (11 per cent higher) and Lagache models (13 per cent lower).

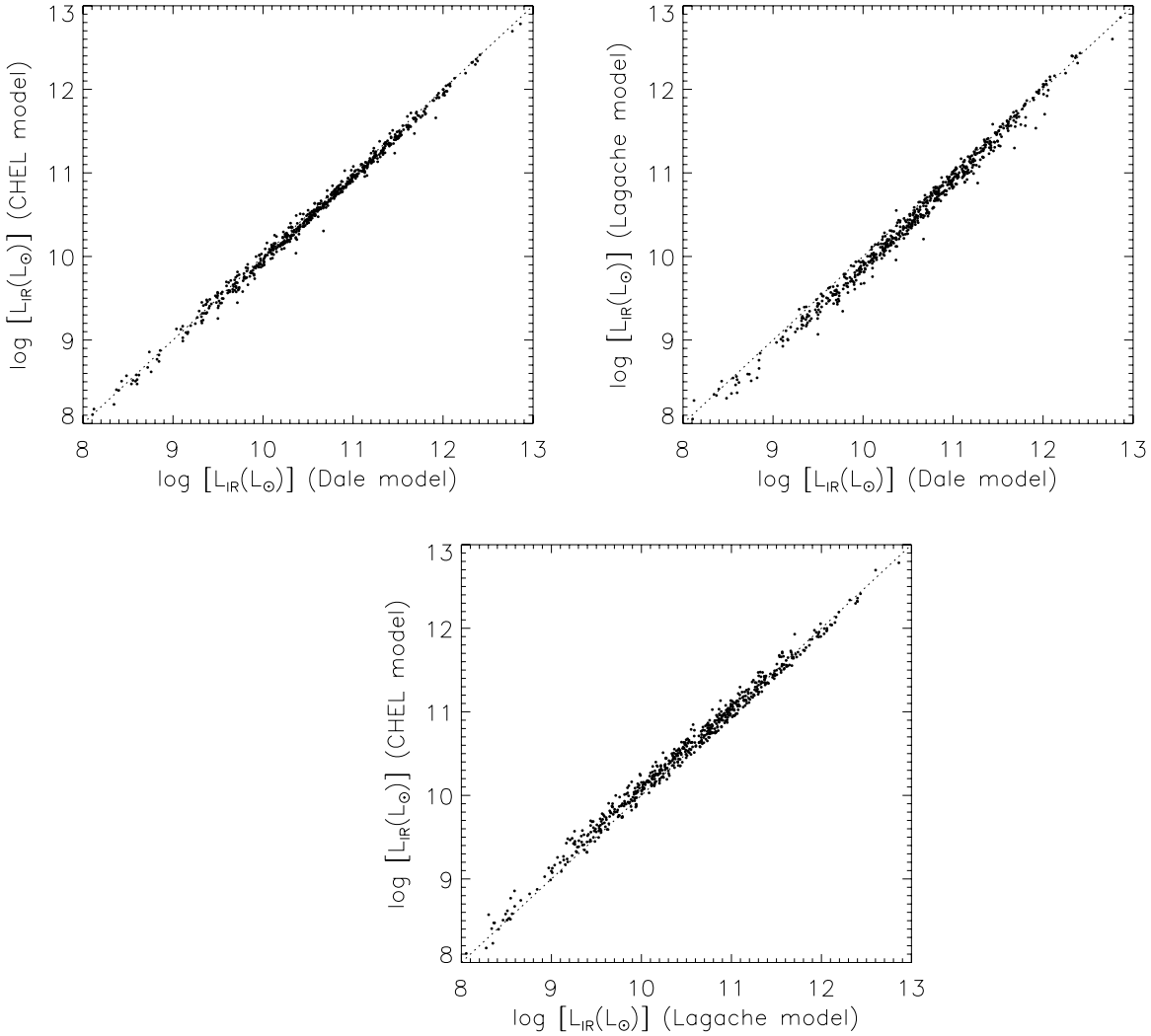

Figure 4. Comparing $L_{\rm TIR}$ measured using three different SED models (Chary & Elbaz 2001; Dale & Helou 2002; Lagache et al. 2003). Scatter and offsets between the models are summarized in Table 1.

Table 1. Comparison of $L_{\rm TIR}$ estimates with different SED models (Chary & Elbaz 2001; Dale & Helou 2002; Lagache et al. 2003). Fig. 4 presents corresponding plots.

Models	σ (per cent)	Offset (per cent)
CHEL versus *IRAS*	44	−23
Dale versus Lagache	24	24
Dale versus CHEL	10	11
Lagache versus CHEL	22	−13

Overall, there are good agreements between models, suggesting that once you have FIR photometry (WL and N160 in this work), the model-dependent uncertainty in $L_{\rm TIR}$ is small. This justifies our use of a single SED library for the final $L_{\rm TIR}$ measurement.

3.3 MIR–$L_{\rm TIR}$ correlation

A good correlation between mid-IR monochromatic luminosity and $L_{\rm TIR}$ is known to exist. This is especially true for SFGs because the rest-frame MIR luminosity is dominated by prominent polycyclic aromatic hydrocarbon (PAH) features such as those at 6.2, 7.7 and 8.6 μm, and the $L_{\rm TIR}$ is by dust emission heated by the SF activity; i.e. both of these are good indicators of SF activity. Observationally MIR detectors are more sensitive than in the FIR. Therefore, if we obtain accurate conversions from MIR to $L_{\rm TIR}$, they will bring $L_{\rm TIR}$ measurement to many more galaxies.

AKARI covers both the MIR and FIR range with its six bandpasses, measuring both MIR and total luminosity well. In addition, because it is an all-sky survey, it provides the six-band photometry for ∼600 RBGS galaxies. Here we have one of the best opportunities to investigate the $L_{\rm MIR}$–$L_{\rm TIR}$ correlation.

We compute the MIR monochromatic luminosity at 8, 9, 12, 15, 18, 22 and 24 μm using the *AKARI* photometry at 9 and 18 μm, and the best-fitting CHEL model from Section 3.1. For precise and easily reproducible definitions of monochromatic luminosity, we chose such luminosities in passbands of existing IR satellites so as to avoid at the same time narrow emission/absorption features that add too much noise to the resulting relation. In addition, this choice allows users to apply the relations easily to observed fluxes, at least for low-redshift galaxies whose *k*-correction is small. We checked and ensured that this choice of monochromatic filters did not have much effect compared to the exact luminosity at a certain single wavelength. We later show that MIR–$L_{\rm TIR}$ correlations for *WISE* 12 μm and *IRAS* 12 μm are almost identical. Our choices of

filters are *Spitzer* 8 μm, *AKARI* 9 μm, *IRAS* 12 μm, *WISE* 12 μm, *ISO* 15 μm, *AKARI* 18 μm, *WISE* 22 μm and *Spitzer* 24 μm.

For $L_{Spitzer\,8\,\mu m}$, $L_{AKARI\,9\,\mu m}$, $L_{IRAS\,12\,\mu m}$ and $L_{WISE\,12\,\mu m}$, we started from the observed 9-μm flux, then used the best-fitting SED (to the six bands) from the CHEL model (Section 3.1) to colour-correct the observed *AKARI* 9-μm flux to $L_{\rm MIR}$ in each filter. To be specific, we computed $L_{Spitzer\,8\,\mu m}$, $L_{AKARI\,9\,\mu m}$, $L_{IRAS\,12\,\mu m}$ and $L_{WISE\,12\,\mu m}$ through the filter response function of the *Spitzer*/IRAC 8 μm, the *AKARI* 9 μm, the *IRAS* 12 μm and *WISE* 12 μm filters. Here, the best-fitting model is only used to colour-correct the observed 9-μm flux, and thus the obtained $L_{\rm MIR}$ is not an integration of flux of the best-fitting model.

Similarly, for $L_{ISO\,15\,\mu m}$, $L_{AKARI\,18\,\mu m}$, $L_{WISE\,22\,\mu m}$ and $L_{Spitzer\,24\,\mu m}$, we started from the observed *AKARI* 18-μm flux, colour-corrected the flux using the colour-correction from the best-fitting SED model in Section 3.1, then converted them to luminosity in each passband. This colour-correction is very small (∼1 per cent at most) because *AKARI*'s 9 and 18 μm are very close to other passbands. Thus, the results in Fig. 5 show almost observed mid-IR luminosity against observed $L_{\rm TIR}$.

In Fig. 5, we show monochromatic luminosity in 8, 9, 12, 15, 18, 22 and 24 μm against $L_{\rm TIR}$ measured using the CHEL model. In Fig. 5, there exist good correlations in each panel. In fact, the correlations look like a simple scaling relation in all panels, i.e. the stronger the MIR-emission, the larger the $L_{\rm TIR}$. The results suggest indeed that monochromatic luminosity in the mid-IR range represents the $L_{\rm TIR}$ well.

We fit a linear equation to the relation obtaining the following results. Note that the unit is in solar luminosity.

The best-fitting relation between $L_{8\,\mu m}$ and $L_{\rm TIR}$ is

$$L_{\rm TIR} = (20 \pm 5) \times \nu L_{\nu,\,8\,\mu m}^{0.94\pm0.01} (\pm 44 \text{ per cent}). \quad (2)$$

The best-fitting relation between $L_{12\,\mu m}$ and $L_{\rm TIR}$ is

$$L_{\rm TIR} = (17 \pm 4) \times \nu L_{\nu,\,12\,\mu m}^{0.96\pm0.01} (\pm 25 \text{ per cent}). \quad (3)$$

The best-fitting relation between $L_{15\,\mu m}$ and $L_{\rm TIR}$ is

$$L_{\rm TIR} = (24 \pm 8) \times \nu L_{\nu,\,15\,\mu m}^{0.96\pm0.01} (\pm 13 \text{ per cent}). \quad (4)$$

The best-fitting relation between $L_{24\,\mu m}$ and $L_{\rm TIR}$ is

$$L_{\rm TIR} = (51 \pm 19) \times \nu L_{\nu,\,24\,\mu m}^{0.91\pm0.01} (\pm 24 \text{ per cent}). \quad (5)$$

The logarithmic slopes of the relations are very similar to each other, perhaps reflecting the fact that most of these IR filters are wide and have some overlaps in wavelength coverage. This also means in this wavelength range (8–24 μm), and within broad filters, the SED shape does not depend much on $L_{\rm TIR}$. However, this result is at low redshift, and whether this applies at a higher redshift needs to be examined separately. We note that $L_{\nu,\,15\,\mu m}$ shows a less dispersed relation with $L_{\rm TIR}$.

For $L_{8\,\mu m}$, Caputi et al. (2007) (equation 6), Bavouzet et al. (2008) (equation 7) and Boquien et al. (2010) (equation 8) each present a correlation:

$$L_{\rm TIR} = 1.91 \times (\nu L_{\nu})_{\rm rest\,8\,\mu m}^{1.06} (\pm 55 \text{ per cent}), \quad (6)$$

$$L_{\rm TIR} = 377.9 \times (\nu L_{\nu})_{\rm rest\,8\,\mu m}^{0.83} (\pm 37 \text{ per cent}), \quad (7)$$

$$L_{\rm TIR} = 216.9 \times (\nu L_{\nu})_{\rm PAH\,8\,\mu m}^{0.836} (\pm 29 \text{ per cent}). \quad (8)$$

Note that for Boquien et al. (2010), we used their conversion in table 1 from SINGS data. The unit is also converted from W to $L_{\odot}$. We overplot these relations in Fig. 5. There is good agreement between these conversions and our best-fitting relation, especially at $9 < \log L_{\rm TIR} < 11$, where both samples have a large enough number of galaxies. Note that Caputi et al. (2007)'s sample spans $0 < z < 0.6$ and Bavouzet et al. (2008)'s is mostly at $z \leq 0.4$. Thus, these samples are significantly at higher redshifts than ours. SED evolution could cause a small difference. See Boquien et al. (2010) for metallicity dependence of the conversion.

For $L_{12\,\mu m}$, there exists a conversion from Takeuchi et al. (2005):

$$\log L_{\rm TIR} = 1.02 + 0.972 \log L_{12\,\mu m}. \quad (9)$$

We overplot the relation in Fig. 5. The slope is in good agreement. There is a ∼50 per cent offset at zero points. The possible reasons for these offsets include the different definition in $L_{12\,\mu m}$ and the different estimates for $L_{\rm TIR}$. Our $L_{12\,\mu m}$ relation is virtually identical to the one given by Spinoglio et al. (1995) which is, in our units,

$$\log L_{\rm TIR} = 1.51 + 0.942 \log L_{12\,\mu m}. \quad (10)$$

For $L_{24\,\mu m}$, we compare the conversions with the following in the literature (Bavouzet et al. 2008; Boquien et al. 2010):

$$L_{\rm TIR} = 57.9 \times (\nu L_{\nu})_{24\,\mu m}^{0.923} (\pm 54 \text{ per cent}), \quad (11)$$

$$L_{\rm TIR} = 6856 \times (\nu L_{\nu})_{24\,\mu m}^{0.71} (\pm 54 \text{ per cent}). \quad (12)$$

Our conversion is in very good agreement with Boquien et al. (2010). Bavouzet et al. (2008)'s relation has a slightly shallower slope, but is in good agreement at $9 < \log L_{\rm TIR} < 11$, where most of their galaxies lie.

Smith et al. (2007) observed 17-μm PAH complex features in *Spitzer* IRS spectra of nearby star-forming galaxies. This feature was not detected previously with *ISO*, and therefore not included in the SED model we used. Although Smith et al. (2007)'s SED templates only contained two data points in the far-IR, and thus were not suitable for our purpose, we try to estimate how the 17-μm PAH complex features affect the $L_{15\,\mu m}$–$L_{\rm TIR}$ conversion as follows. First, we remove a continuum from both of the spectra (Chary & Elbaz 2001; Smith et al. 2007). Then we replace the 6–20 μm region of the Chary & Elbaz (2001) spectra by Smith et al. (2007)'s. Here we scaled the spectrum so that the amplitude of the 12-μm PAH complex matches. Thus, these new templates retain the overall SED shape of Chary & Elbaz (2001), but have the 17-μm PAH complex features from Smith et al. (2007). We rerun the SED fit to estimate the $L_{15\,\mu m}$–$L_{\rm TIR}$ conversion to find that the $L_{\rm TIR}$ estimate (as a function of $L_{15\,\mu m}$) will be ∼3 per cent smaller if the 17-μm PAH complex features are included in the SED. Although the effect is smaller than the errors of the conversion, this indicates that future SED models need to include the 17-μm PAH complex features.

With current technology, detectors are much more sensitive in the mid-IR range than in the far-IR range. Therefore, once these correlations are assumed, they will provide a useful conversion to compute luminosities of many more galaxies, either at higher redshift or at a fainter flux level, from a single MIR flux. For example, the above relations can provide a total IR flux measurement for all sources from the *AKARI* MIR all-sky survey, which has three times more sources than the FIR all-sky survey. *WISE* will perform an even deeper all-sky survey in 3.4, 4.6, 12 and 22 μm in the near future (Wright 2008). For future use, we also provide $L_{12\,\mu m}$–$L_{\rm TIR}$ and $L_{22\,\mu m}$–$L_{\rm TIR}$ conversions in *WISE* filters as follows, and also in Fig. 5.

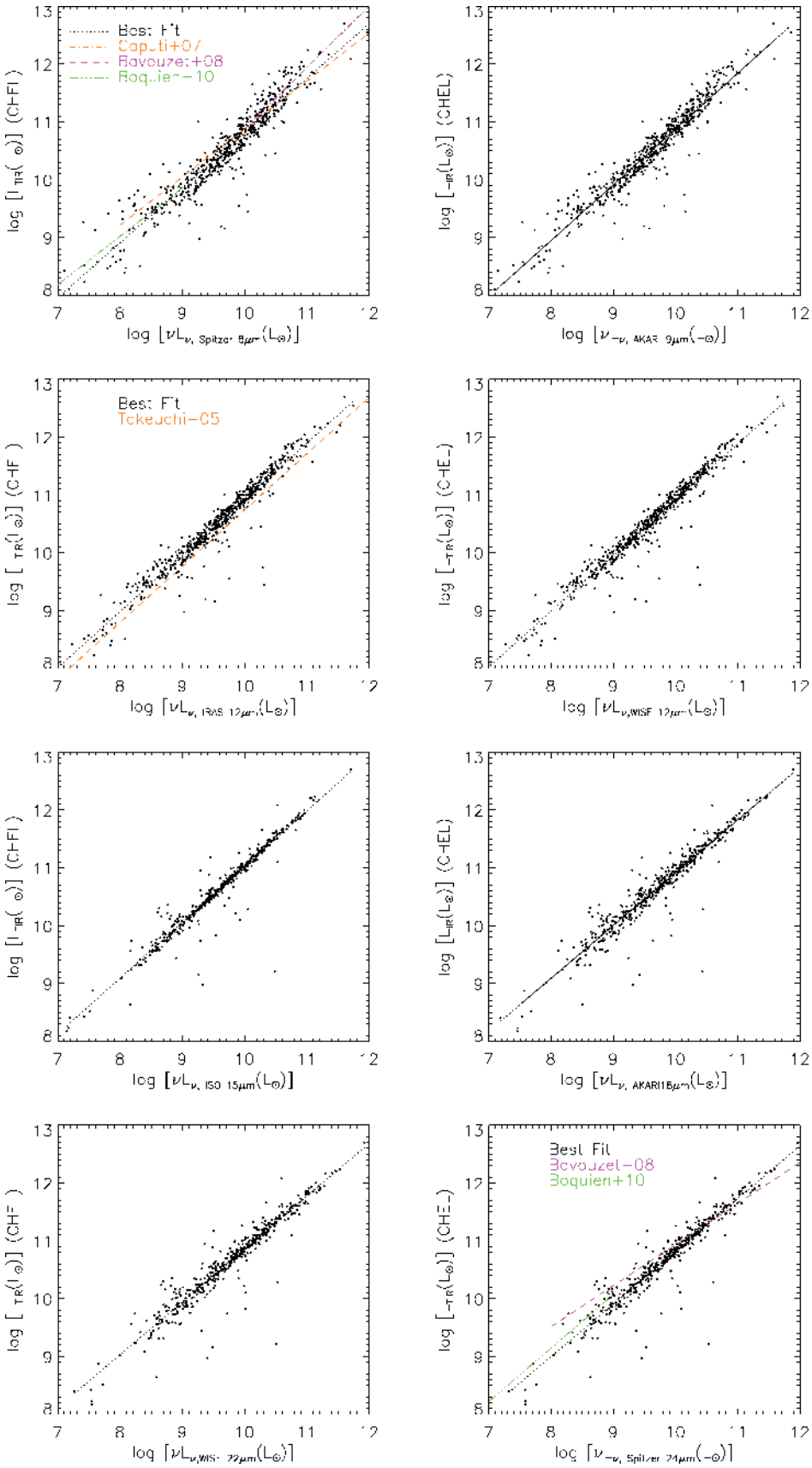

Figure 5. Correlations between $L_{\rm TIR}$ and monochromatic luminosities (8, 9, 12, 15, 18, 22 and 24 μm). The lines show the best-fitting polynomial, based on which we present conversions. When available, conversions from the literature (Takeuchi et al. 2005; Caputi et al. 2007; Bavouzet et al. 2008; Boquien et al. 2010) are overplotted for a comparison.

The best-fitting relation between $L_{WISE\,12\,\mu m}$ and L_{TIR} is

$$L_{TIR} = (18 \pm 5) \times \nu L_{\nu,WISE\ 12\,\mu m}^{0.96\pm0.01} (\pm 23 \text{ per cent}). \quad (13)$$

The best-fitting relation between $L_{WISE\,22\,\mu m}$ and L_{TIR} is

$$L_{TIR} = (53 \pm 20) \times \nu L_{\nu,WISE\,22\,\mu m}^{0.91\pm0.01} (\pm 25 \text{ per cent}). \quad (14)$$

4 INFRARED LUMINOSITY FUNCTIONS

4.1 The $1/V_{max}$ method

With accurately measured L_{TIR}, we are ready to construct IR LFs. Since the RBGS is a flux-limited survey, we need to correct for a volume effect to compute LFs. We used the $1/V_{max}$ method (Schmidt 1968) for this. An advantage of the $1/V_{max}$ method is that it allows us to compute an LF directly from data, with no parameter dependence or a model assumption. A drawback is that it assumes a homogeneous galaxy distribution and thus is vulnerable to local over-/under-densities (Takeuchi, Yoshikawa & Ishii 2000).

A comoving volume associated with any source of a given luminosity is defined as $V_{max} = V_{z_{max}} - V_{z_{min}}$, where z_{min} is the lower limit of the redshift and z_{max} is the maximum redshift at which the object could be seen given the flux limit of the survey. In this work, we set $z_{min} = 0.0004$ since at a very small redshift, an error in redshift measurement is dominated by a peculiar motion, and thus, L_{TIR} also has a large error. This only removes five galaxies from the sample.

For the RBGS, the detection limit is *IRAS* $S_{60\,\mu m} = 5.24$ Jy. We used the SED templates (Chary & Elbaz 2001) for k-correction to obtain the maximum observable redshift from the flux limit.

For each luminosity bin then, the LF is derived as

$$\phi = \frac{1}{\Delta L} \sum_i \frac{1}{V_{max,i}}, \quad (15)$$

where V_{max} is a comoving volume over which the ith galaxy could be observed, and ΔL is the size of the luminosity bin (0.3 dex). The RBGS is complete in 60 μm at *IRAS* $S_{60\,\mu m} > 5.24$ Jy. Completeness correction in terms of sky coverage of both satellites is taken into account.

4.2 Monte Carlo simulation

Uncertainties in the LF values stem from various factors such as the finite numbers of sources in each luminosity bin, the k-correction uncertainties and the flux errors. To compute these errors we performed Monte Carlo simulations by creating 1000 simulated catalogues, where each catalogue contains the same number of sources, but we assign each source new fluxes following a Gaussian distribution centred at fluxes with a width of a measured error. Then we measured errors of each bin of the LF based on the variation in the 1000 simulations. These estimated errors are added in quadrature to the Poisson errors in each LF bin.

4.3 IR luminosity function

In Fig. 6, we show LF of the RBGS obtained using *AKARI* photometry. Fig. 7 shows the number of galaxies used to compute the LF. The original LF measured using the *IRAS* photometry is also overplotted. There is a very good agreement between the LFs measured by *AKARI* and *IRAS* over the luminosity range of $8 < \log L_{TIR} < 12$. Although the *IRAS*-based L_{TIR} is computed using a single polynomial equation (equation 1), the agreement shows it measured the

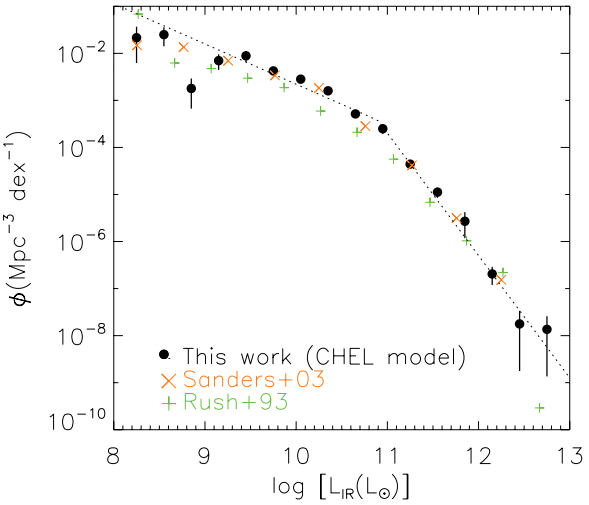

Figure 6. Infrared luminosity function of the RBGS. The L_{TIR} is measured using the *AKARI* 9, 18, 65, 90, 140 and 160 μm fluxes through an SED fit. Errors are computed using 1000 Monte Carlo simulations, added by Poisson error. The dotted lines show the best-fitting double-power law. The crosses show data from Sanders et al. (2003), who measured L_{TIR} using *IRAS* photometry. The pluses show data from Rush et al. (1993), who measured L_{FIR} by integrating *IRAS* fluxes over 12–100 μm.

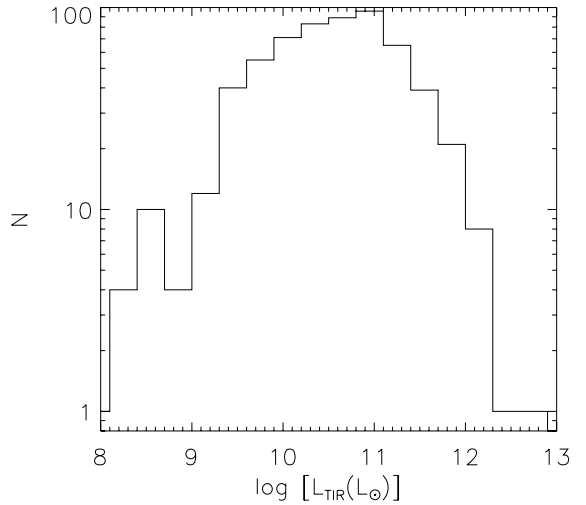

Figure 7. A luminosity histogram of galaxies used to compute Fig. 6.

IR LF very well. Perhaps, since an LF is an integrated quantity, it can be measured more reliably than L_{TIR} of individual galaxies, even using data up to only 100 μm.

Our LF in Fig. 6 agrees well with Rush, Malkan & Spinoglio (1993), after correcting their results from a Hubble constant of 50–75. Their LF slightly underestimate LF, perhaps because they only integrated *IRAS* photometry up to 100 μm. Our LF also agrees well with Takeuchi, Yoshikawa & Ishii (2003) once their 60-μm LF is converted to L_{TIR} by multiplying by 2.5 (Takeuchi et al. 2006). Their LF was measured in an SED model-free way, using different density estimators. It is reassuring that LFs measured in completely different ways agree well. See Sedgwick et al. (2010) for a similar attempt in the *AKARI Deep Field*-South.

Following Sanders et al. (2003), we fit an analytical function to the LFs. In the literature, IR LFs were fitted better by a

Table 2. Best double-power law fit parameters for the *AKARI* LFs, and the infrared luminosity density obtained from the fit.

Sample	$L^*_{\rm TIR}$ ($L_\odot$)	ϕ^*(Mpc^{-3}dex^{-1})	α (faint-end)	β (bright-end)	$\Omega_{\rm IR}$($L_\odot$Mpc^{-3})
Total	$7.8 \pm 0.2 \times 10^{10}$	0.00037 ± 0.00005	1.8 ± 0.1	3.6 ± 0.1	$8.5^{+1.5}_{-2.3} \times 10^7$
SFG	$10 \pm 0.2 \times 10^{10}$	0.00018 ± 0.00006	1.9 ± 0.1	4.4 ± 0.3	$8.0^{+1.7}_{-2.5} \times 10^7$
AGN	$7.8 \pm 0.2 \times 10^{10}$	0.00011 ± 0.00005	1.7 ± 0.1	3.2 ± 0.3	$1.6^{+0.5}_{-0.3} \times 10^7$

double-power law (Babbedge et al. 2006; Goto et al. 2010) or a double-exponential (Saunders et al. 1990; Pozzi et al. 2004; Le Floc'h et al. 2005; Takeuchi et al. 2006) than by a Schechter function, which steeply declines at high luminosity and underestimates the number of bright galaxies. In this work, we fit the TIR LFs using a double-power law (Babbedge et al. 2006):

$$\Phi(L){\rm d}L/L^* = \Phi^* \left(\frac{L}{L^*}\right)^{1-\alpha} {\rm d}L/L^*, \qquad L < L^*, \tag{16}$$

$$\Phi(L){\rm d}L/L^* = \Phi^* \left(\frac{L}{L^*}\right)^{1-\beta} {\rm d}L/L^*, \qquad L > L^*. \tag{17}$$

Free parameters are L^* (characteristic luminosity, $L_\odot$); ϕ^* (normalization, Mpc^{-3}); α; and β (faint and bright end slopes), respectively. The best-fitting values are summarized in Table 2. The local LF has a break at $L^* = 7.8 \pm 0.2 \times 10^{10}$. Understanding how this break (L^*) evolves as a function of cosmic time, and what causes the break, is fundamental to galaxy evolution studies. This work provides an important benchmark in the local Universe.

4.4 Bolometric IR luminosity density based on the TIR LF

One of the primary purposes in computing IR LFs is to estimate the IR luminosity density, which is in turn a good estimator of the dust-hidden cosmic star formation density (Kennicutt 1998), provided the AGN contribution is removed. The bolometric IR luminosity of a galaxy is produced by thermal emission of its interstellar matter. In SF galaxies, the UV radiation produced by young stars heats the interstellar dust, and the reprocessed light is emitted in the IR. For this reason, in star-forming galaxies (SFGs), the bolometric IR luminosity is a good estimator of the current SFR (star formation rate) of the galaxy.

Once we measured the LF, we can estimate the total infrared luminosity density by integrating the LF, weighted by the luminosity. We used the best-fitting double-power law to integrate outside the luminosity range in which we have data, to obtain estimates of the total infrared luminosity density, $\Omega_{\rm TIR}$.

The resulting total luminosity density is $\Omega_{\rm TIR} = (8.5^{+1.5}_{-2.3}) \times 10^7\,{\rm L}_\odot\,{\rm Mpc}^{-3}$. Errors are estimated by varying the fit within 1σ of uncertainty in LFs. Out of $\Omega_{\rm TIR}$, 7 ± 1 per cent is produced by luminous infrared galaxies (LIRGs) ($L_{\rm TIR} > 10^{11}\,{\rm L}_\odot$), and only 0.4 ± 0.1 per cent is by ultraluminous infrared galaxies (ULIRGs) ($L_{\rm TIR} > 10^{12}\,{\rm L}_\odot$). A very small fraction of $\Omega_{\rm TIR}$ is produced by luminous infrared galaxies at $z = 0.0082$, in stark contrast to the high-redshift Universe. We have found that $\sim$30 per cent of $\Omega_{\rm TIR}$ originates from $L_{\rm TIR} < 10^{8.2}\,{\rm L}_\odot$, where we do not have data and had to rely on the extrapolation of the faint-end tail of the LF. Therefore, a similar amount of uncertainty cannot be ruled out if the faint-end slope changes significantly under $L_{\rm TIR} < 10^{8.2}\,{\rm L}_\odot$. We will discuss the evolution of $\Omega_{\rm TIR}$ in Section 5.2.

5 INFRARED LUMINOSITY DENSITY AND ITS EVOLUTION

5.1 Separating IR contributions from AGN and SFGs

We showed a local IR LF in Fig. 6. However, this includes IR emission both from star formation activity and from AGN. Since different physics govern star formation and AGN, it is essential to separate their IR emission to understand the cosmic evolution of each component. For example, the cosmic star formation history cannot be addressed without subtracting the contribution from the AGN, and vice versa.

Separating AGN from starbursts is not a trivial task. Many AGN/SF separation methods have been proposed, such as X-ray, radio luminosity, optical line ratios, PAH strengths, submillimetre properties and so on, many of which often disagree with the others. We do not have a complete diagnosis of AGN/starburst, such as emission line ratios and X-rays, for all of our samples. Therefore, instead of classifying individual galaxies into AGN and SF, we attempt a statistical approach to separate contributions to LFs by AGN and SFGs.

In this work, we simply use the result of a new classification system proposed by Yuan, Kewley & Sanders (2010), which uses three carefully examined optical line ratio diagrams (Kewley et al. 2006) to classify individual galaxies. Based on optical line ratios, they classify IR galaxies into AGN (LINER, Seyfert 1 and 2), star forming and composite as a function of $L_{\rm TIR}$ in their table 4 and fig. 4. Their results agree well with other works (Takeuchi et al. 2003; Goto 2005), within 20 per cent or so. We use their fractions of AGN/SFGs as a function of $L_{\rm TIR}$, to separate our LF into that of AGN and SFGs. In this process, it is an open question as to how to handle composite galaxies, which are close to 50 per cent of galaxies in almost all bins. In this work, we simply assigned the AGN/SF fractional ratio of that luminosity bin to separate composite galaxies (and ambiguous galaxies) into AGN/SF galaxies. We understand this is not an ideal approach. There will be up to $\sim$50 per cent uncertainty if these composite galaxies are all AGN or SFGs. It merely provides one method to separate IR LFs into those of AGN and SFGs. A method to assess IR contribution by AGN and SFGs is becoming realistic. For example, Gandhi et al. (2009) showed a tight correlation between nuclear $L_{12.3\,\mu{\rm m}}$ and $L_{\rm X\text{-}ray}$. In the near future, more realistic classification of composite galaxies will become possible. We show the resulting AGN fraction from this process as a function of $L_{\rm TIR}$ in Fig. 8. At $L_{\rm TIR} > 10^{12}\,{\rm L}_\odot$, this procedure assigns 90 per cent of IR luminosity to AGN. At $L_{\rm TIR} < 10^{10}\,{\rm L}_\odot$, the AGN fraction is 20 per cent or less. This also agrees well with a recent measurement by Kartaltepe et al. (2010).

By applying this AGN/SF separation, in Fig. 9 we show LFs separately for AGN and SFGs. The total IR LF shown in Fig. 6 is also shown for comparison. As expected, Figs 8 and 9 show that at $L_{\rm TIR} > 10^{12}\,{\rm L}_\odot$, the AGN are responsible for almost all of the $L_{\rm TIR}$, forming a very steep bright-end drop for the SFG LF. On the other hand, at $L_{\rm TIR} < 10^{11}\,{\rm L}_\odot$, SF galaxies explain most of the $L_{\rm TIR}$.

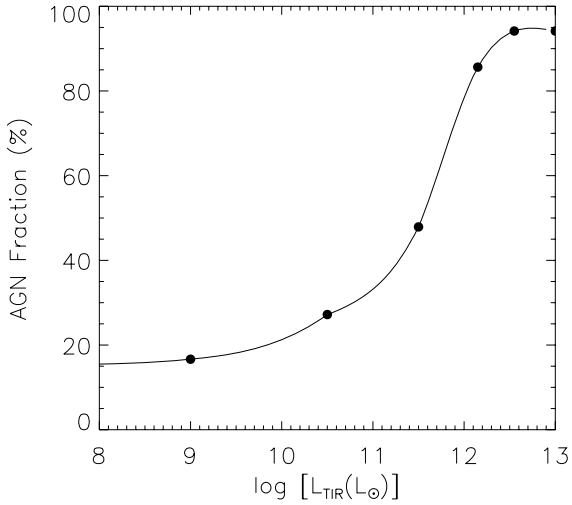

Figure 8. Fractions of AGN are shown as a function of $L_{\rm TIR}$. The original classification was taken from fig. 4 of Yuan et al. (2010), and interpolated by a spline curve to be applied to our LFs.

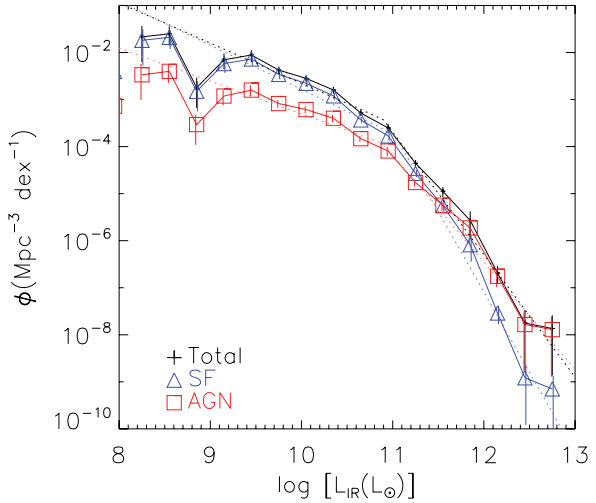

Figure 9. The IR LF is separated for SFGs (blue triangles) and AGN (red squares) using Fig. 8. Total IR LF is shown with the black plus sign. The dotted lines are the best-fitting double-power laws.

Next, we fit a double-power law (equations 16 and 17) to the AGN and SF IR LFs, exactly as we did for the total IR LF in Fig. 6. The best-fitting parameters are summarized in Table 2. The most notable difference is at the bright-end slope (β), where the AGN LF has a very shallow slope of $\beta = 3.2 \pm 0.3$, while the SFG has a steep slope of $\beta = 4.4 \pm 0.3$. As expected, the faint-end tail (α) is not much different, in fact, being consistent with each other within 1σ. The L^* of SFG becomes brighter due to the steepening of the bright-end slope.

The total infrared luminosities of AGN and SFGs were also measured in separate LFs by Rush et al. (1993). Adding their Seyfert 1 and Seyfert 2 LFs, and correcting for different Hubble constants, they get somewhat lower AGN/SFG LF ratios than our overall value of 1.6:8.0. Their methodology was simpler, and did not account for the population of LINER AGN in their 12-μm-selected galaxy sample.

What do these differences in LFs bring to the IR luminosity density, $\Omega_{\rm IR}$, by AGN and SFGs? We estimate the total infrared luminosity density by integrating the LFs weighted by the luminosity, separately for AGN and SFGs. We used the double-power law outside the luminosity range in which we have data, to obtain estimates of the total infrared luminosity density, $\Omega_{\rm TIR}$, for AGN and SFGs.

Table 3. Local IR luminosity densities.

Sample	$\Omega_{\rm IR}^{\rm SFG}$ ($L_\odot$ Mpc^{-3})	$\Omega_{\rm IR}^{\rm AGN}$ ($L_\odot$ Mpc^{-3})
Total	$(8.0^{+1.7}_{-2.5}) \times 10^7$	$(1.6^{+0.5}_{-0.3}) \times 10^7$
LIRG	$(3.8^{+0.4}_{-0.9}) \times 10^6$	$(2.1^{+0.6}_{-0.5}) \times 10^6$
ULIRG	$(1.5^{+1.0}_{-1.0}) \times 10^4$	$(12^{+5}_{-7}) \times 10^4$

The resulting $\Omega_{\rm IR}$ is $\Omega_{\rm IR}^{\rm SFG} = 8.0^{+1.7}_{-2.5} \times 10^7\,{\rm L}_\odot\,{\rm Mpc}^{-3}$, and $\Omega_{\rm IR}^{\rm AGN} = 1.6^{+0.5}_{-0.3} \times 10^7\,{\rm L}_\odot\,{\rm Mpc}^{-3}$, as summarized in Table 3. Errors are estimated by varying the fit within 1σ of uncertainty in LFs. These are also summarized in Table 2. The results show that among the total IR luminosity density integrated over all the IR luminosity range, 83 per cent $[\Omega_{\rm IR}^{\rm SFG}/(\Omega_{\rm IR}^{\rm AGN} + \Omega_{\rm IR}^{\rm SFG})]$ of IR luminosity density is emitted by the SFGs, and only 16 per cent $[\Omega_{\rm IR}^{\rm AGN}/(\Omega_{\rm IR}^{\rm AGN} + \Omega_{\rm IR}^{\rm SFG})]$ is by AGN at $z = 0.0082$. The results show that at low redshift ($z = 0.0082$), the majority of the IR luminosity density is emitted by the SFGs. Therefore, even if you convert all the $\Omega_{\rm IR}$ into SFR density, you will only overestimate by 20 per cent. However, the situation is different at a higher redshift, where a number of papers reported luminosity evolution in the IR LF (Le Floc'h et al. 2005; Pérez-González et al. 2005; Magnelli et al. 2009). The AGN/SFG separation will have an effect that is much larger and therefore more important at higher redshift.

Once we have $\Omega_{\rm IR}^{\rm SFG}$, we can estimate the star formation density emitted in infrared light. The SFR and $L_{\rm TIR}$ are related by the following equation for a Salpeter initial mass function, $\phi(m) \propto m^{-2.35}$ between 0.1 and 100 $\rm M_\odot$ (Kennicutt 1998):

$$\mathrm{SFR}\,(\mathrm{M}_\odot\,\mathrm{yr}^{-1}) = 1.72 \times 10^{-10} L_{\rm TIR}\,(\mathrm{L}_\odot). \quad (18)$$

By using this equation, we obtain the SFR density $1.3 \pm 0.2 \times 10^{-2}\,{\rm M}_\odot\,{\rm yr}^{-1}$.

If we limit our integration to the ULIRG luminosity range ($L_{\rm TIR} > 10^{12}\,{\rm L}_\odot$), we obtain $\Omega_{\rm IR}^{\rm SFG}({\rm ULIRG}) = (1.5^{+1.0}_{-1.0}) \times 10^4\,{\rm L}_\odot\,{\rm Mpc}^{-3}$, and $\Omega_{\rm IR}^{\rm AGN}({\rm ULIRG}) = (12^{+5}_{-7}) \times 10^4\,{\rm L}_\odot\,{\rm Mpc}^{-3}$. In other words, at ULIRG luminosity range, AGN explain 88 per cent $[\Omega_{\rm IR}^{\rm AGN}({\rm ULIRG})/(\Omega_{\rm IR}^{\rm AGN}({\rm ULIRG}) + \Omega_{\rm IR}^{\rm SFG}({\rm ULIRG}))]$ of IR luminosity, again showing the AGN dominance at the bright end.

In the LIRG luminosity range ($L_{\rm TIR} > 10^{11}\,{\rm L}_\odot$), the results are $\Omega_{\rm IR}^{\rm SFG}({\rm LIRG}) = (3.8^{+0.4}_{-0.9}) \times 10^6\,{\rm L}_\odot\,{\rm Mpc}^{-3}$, and $\Omega_{\rm IR}^{\rm AGN}({\rm LIRG}) = (2.1^{+0.6}_{-0.5}) \times 10^6\,{\rm L}_\odot\,{\rm Mpc}^{-3}$. This shows that the AGN contribution is already down to 35 per cent $[\Omega_{\rm IR}^{\rm AGN}({\rm LIRG})/(\Omega_{\rm IR}^{\rm AGN}({\rm ULIRG}) + \Omega_{\rm IR}^{\rm SFG}({\rm LIRG}))]$ of IR luminosity in the LIRG range.

5.2 Evolution of $\Omega_{\rm IR}^{\rm SFG}$

We have separated the $\Omega_{\rm IR}^{\rm SFG}$ from $\Omega_{\rm IR}^{\rm AGN}$. Now we are ready to examine the evolution of $\Omega_{\rm SFR}$ without contribution from AGN. In Fig. 10, we plot the evolution of $\Omega_{\rm IR}^{\rm SFR}$ as a function of redshift. Higher-redshift results are taken from Goto et al. (2010), who also tried to exclude AGN using SED fitting to individual galaxies. Results from the *Spitzer* survey and *GALEX* survey are also plotted. The $\Omega_{\rm IR}^{\rm SFG}$ shows a strong evolution as a function of redshift. The best-fitting linear relation is $\Omega_{\rm IR}^{\rm SFG} \propto (1+z)^{4.0\pm0.5}$. This is consistent with most earlier work. For example, Le Floc'h et al. (2005) obtained $\gamma = 3.9 \pm 0.4$ up to $z \sim 1$. Pérez-González et al. (2005)

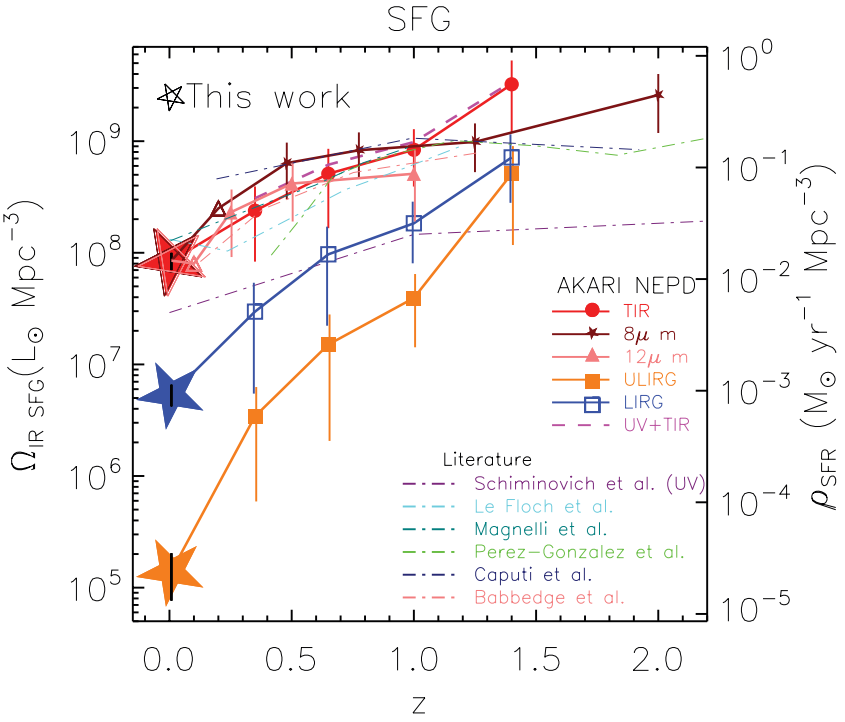

Figure 10. Evolution of TIR luminosity density by star-forming galaxies. Results from this work are plotted with triangles at $z = 0.0082$. The red, blue and orange triangles show IR luminosity density from all galaxies, from LIRGs only, and from ULIRGs only. Higher-redshift results in the solid lines are from the *AKARI* NEP deep field (Goto et al. 2010). Shown with different colours are TIR luminosity density based on TIR LFs (red circles), 8-μm LFs (stars) and 12-μm LFs (filled triangles). The blue open squares and orange filled squares are for only LIRGs and ULIRGs, also based on our L_{TIR} LFs. Overplotted dot–dashed lines are estimates from the literature: Le Floc'h et al. (2005), Magnelli et al. (2009), Pérez-González et al. (2005), Caputi et al. (2007) and Babbedge et al. (2006) are in cyan, yellow, green, navy and pink, respectively. The purple dash–dotted line shows the UV estimate by Schiminovich et al. (2005). The pink dashed line shows the total estimate of IR (TIR LF) and UV (Schiminovich et al. 2005).

found $\gamma = 4.0 \pm 0.2$ from $z = 0$ to 0.8. Babbedge et al. (2006) obtained $\gamma = 4.5^{+0.7}_{-0.6}$. Magnelli et al. (2009) obtained $\gamma = 3.6 \pm 0.4$ up to $z = 1.3$. Rodighiero et al. (2010) found $\gamma = 3.8 \pm 0.4$ in the redshift interval of $0 < z < 1$. Gruppioni et al. (2010) found $\gamma = 3.8 \pm 0.3$ up to $z \sim 1$, with some evidence of flattening up to $z \sim 2$.

Once the IR luminosity density was separated into ULIRG and LIRG contributions, we found $\Omega_{IR}^{SFG}(\mathrm{ULIRG}) \propto (1+z)^{9.1\pm0.8}$, and $\Omega_{IR}^{SFG}(\mathrm{LIRG}) \propto (1+z)^{5.3\pm2.0}$. $\Omega_{IR}^{SFG}(\mathrm{ULIRG})$ shows more rapid evolution than $\Omega_{IR}^{SFG}(\mathrm{LIRG})$, showing the importance of luminous IR sources at high redshift.

5.3 Evolution of Ω_{IR}^{AGN}

In turn, we can also investigate the evolution of Ω_{IR}^{AGN}. This has been difficult in the literature since it is difficult to separate faint AGN individually in the presence of a host galaxy. By integrating IR $\mathrm{LF_{AGN}}$ in Fig. 9, we obtained $\Omega_{IR}^{AGN} = 1.6^{+0.5}_{-0.3} \times 10^7\ L_\odot\ \mathrm{Mpc}^{-3}$.

Kartaltepe et al. (2010) recently reported that the mean SED of the 70-μm-selected sample from the COSMOS survey at $z \sim 1$ is similar to what has been observed locally. As a natural consequence, the fraction of AGN as a function of L_{IR} is in excellent agreement with that in the local Universe (their fig. 30). If so, we can apply the f_{AGN}–L_{IR} relation described in Fig. 8 to IR LFs at higher redshifts to investigate the evolution of Ω_{IR}^{AGN}.

Practically, we applied the f_{AGN}–L_{IR} relation in Fig. 8 to IR LFs at $0 < z < 1.5$ presented by Goto et al. (2010) to obtain Ω_{IR}^{AGN}. Goto et al. (2010) used their own AGN/SFG classification to remove AGN from their LFs, but for a fair comparison, we applied the same methodology as used in Section 5.1 to their LFs before they subtract the contribution from individual AGN.

In Fig. 11, we show the evolution of Ω_{IR}^{AGN}, which shows a strong evolution with increasing redshift. At a first glance, both Ω_{IR}^{AGN} and Ω_{IR}^{SFG} show rapid evolution, suggesting that the correlation between star formation and black hole accretion rate continues to hold at higher redshifts, i.e. galaxies and black holes seem to be evolving hand in hand. However, there are some differences as well. When we fitted the evolution with $(1+z)^\gamma$, we found $\Omega_{IR}^{AGN} \propto (1+z)^{4.4\pm0.4}$, which is possibly a more rapid evolution than Ω_{IR}^{SFG} although errors are significant. The contribution by ULIRGs quickly increases towards higher redshift; by $z = 1.5$, it exceeds that from LIRGs. Indeed, we found $\Omega_{IR}^{AGN}(\mathrm{ULIRG}) \propto (1+z)^{9.4\pm0.8}$ and $\Omega_{IR}^{AGN}(\mathrm{LIRG}) \propto (1+z)^{5.5\pm0.8}$.

It seems there is no sign of flattening at high redshift in $\Omega_{IR}^{AGN}(z)$. It would be interesting to compare this with a number density evolution of optical QSOs (Croom et al. 2004; Richards et al. 2006), which peaks at $z = 2$–3, and the evolution of X-ray AGN (Ueda et al. 2003; Hasinger, Miyaji & Schmidt 2005). Aird et al. (2010) recently presented the evolution of X-ray luminosity density, which shows a turnover at around $z \sim 1.2 \pm 0.1$. In Fig. 11, our Ω_{IR}^{AGN} does not show any sign of decline at least up to $z = 1.5$, in contrast to the X-ray results. Barger et al. (2005) also showed much shallower evolution in X-ray than our IR results. In Fig. 12, we investigate the evolution of X-ray luminosity density to Ω_{IR}^{AGN} ratio. X-ray luminosity densities are taken from Aird et al. (2010) (2–10 keV) and Hasinger et al. (2005) (0.5–2 keV). It is interesting that the ratio is consistent with a constant value at $0 < z < 1$, and

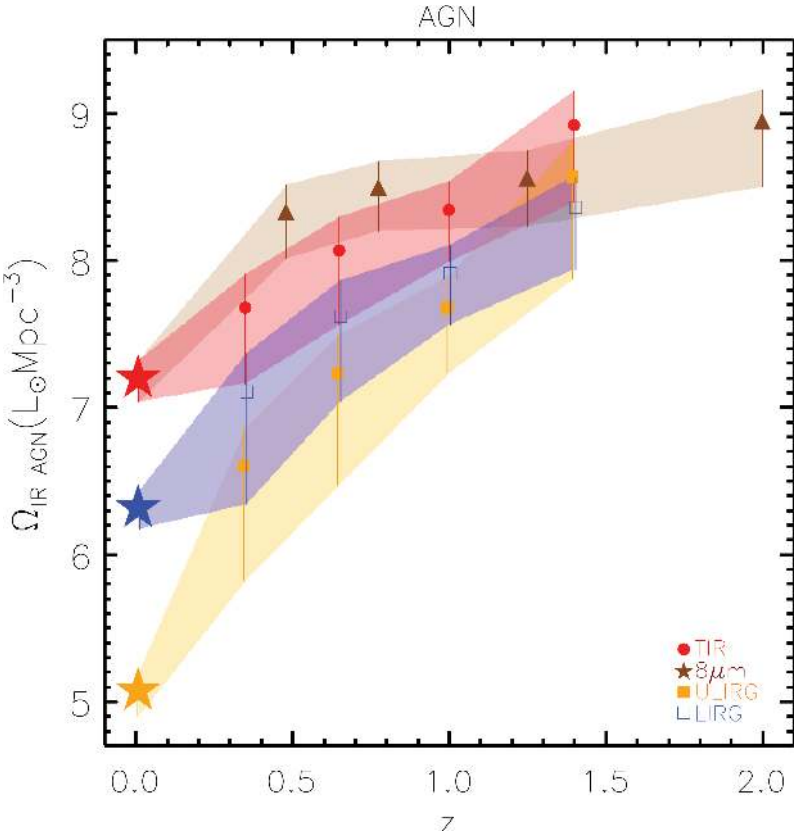

Figure 11. Evolution of TIR luminosity density by AGN. Results from this work are plotted with stars at $z = 0.0082$. The red, blue and orange points show IR luminosity density from all AGN, from LIRG AGN only and from ULIRG AGN only. Higher-redshift results are from the *AKARI* NEP deep field (Goto et al. 2010), with contribution from SFGs removed. Brown triangles are Ω_{IR}^{AGN} computed from the 8-μm LFs (Goto et al. 2010).

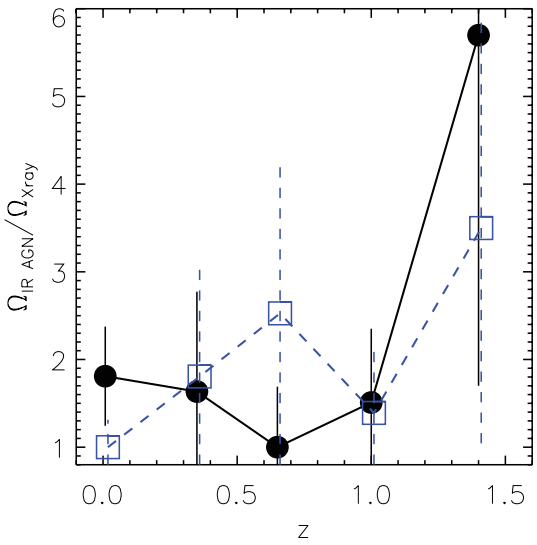

Figure 12. X-ray luminosity density to Ω_{IR}^{AGN} ratio is plotted as a function of redshift. The ratio is normalized at the minimum value. The X-ray luminosity densities of black circles and blue squares are from Aird et al. (2010) (2–10 keV) and Hasinger et al. (2005) (0.5–2 keV), respectively.

shows a possible increase at $z > 1$, although it is unfortunate that our errors are too large for us to draw a firm conclusion. The possible difference may suggest an increase of obscured AGN light towards higher redshift at $z > 1$ compared with optical/X-ray unobscured AGN. Post-starburst AGN galaxies found by Goto (2006) may be an example of such phenomena. Recently, Treister et al. (2010) showed an increase in the number ratio of obscured/unobscured QSOs with increasing redshift, concluding that a merger-driven black hole evolution model is consistent with the observed result. Our Fig. 12 may suggest a similar obscured/unobscured AGN evolution in terms of AGN luminosity density, instead of the number density. A possible deviation from Ω_{IR}^{SFG} also suggests that AGN may have formed earlier than stars in terms of infrared luminosity density. A more accurate comparison of X-ray and IR luminosity density evolution of AGN may reveal some interesting physical implications of the subject. In particular, reducing measurement errors at high redshift is urgent.

6 SUMMARY

Using *AKARI*'s six-band IR photometry at 9, 18, 65, 90, 140 and 160 μm with much improved spatial resolution to resolve background cirrus/confusing sources, we have remeasured L_{TIR} of the RBGS through IR SED model fitting. This is significant progress considering that *IRAS* used one linear equation to estimate L_{TIR}, with the only data being at <100 μm.

By using this new L_{TIR} measurement, we have constructed local IR LFs separately for SFGs and AGN. We have also computed local infrared luminosity density through the derived LFs, and compared Ω_{IR}^{SFG} and Ω_{IR}^{AGN} to those at higher redshifts.

Our findings are as follows.

(i) SED model-to-model variation in estimating L_{TIR} is less than 25 per cent.

(ii) We present $L_{\rm MIR}$-to-$L_{\rm TIR}$ conversions for *Spitzer* 8 μm, *AKARI* 9 μm, *IRAS* 12 μm, *WISE* 12 μm, *ISO* 15 μm, *AKARI* 18 μm, *WISE* 22 μm and *Spitzer* 24 μm filters. These conversions provide us with a useful tool to estimate $L_{\rm TIR}$ with an MIR band only.

(iii) A reconstructed local TIR LF with the *AKARI* data is consistent with that from *IRAS*, i.e. *AKARI*'s better data show that the *IRAS* measurement was correct.

(iv) By integrating the IR LF weighted by $L_{\rm TIR}$, we obtain the local cosmic IR luminosity density of $\Omega_{\rm TIR} = (8.5^{+1.5}_{-2.3}) \times 10^7\,{\rm L}_\odot\,{\rm Mpc}^{-3}$.

(v) LIRGs and ULIRGs contribute to $\Omega_{\rm TIR}$ a little: only 7 ± 1 per cent of $\Omega_{\rm TIR}$ is produced by LIRGs ($L_{\rm TIR} > 10^{11}\,{\rm L}_\odot$), and only 0.4 ± 0.1 per cent is by ULIRGs ($L_{\rm TIR} > 10^{12}\,{\rm L}_\odot$) in the local Universe, in stark contrast to high-redshift results.

(vi) Compared with high-redshift results from the *AKARI* NEP deep survey, we observed a strong evolution of $\Omega_{\rm TIR}^{\rm SFG} \propto (1+z)^{4.0\pm0.5}$, after removing the AGN contribution.

(vii) We show that the evolution of $\Omega_{\rm IR}^{\rm AGN}$ scales as $\propto (1+z)^{4.4\pm0.4}$. The ULIRG contribution to the $\Omega_{\rm IR}^{\rm AGN}$ exceeds that by LIRGs by $z = 1.5$.

(viii) The $\Omega_{\rm IR}^{\rm AGN}/\Omega_{\rm X-ray}^{\rm AGN}$ ratio shows a possible increase at $z > 1$. If confirmed, this may suggest an increase of obscured AGN at $z > 1$.

ACKNOWLEDGMENTS

We thank the anonymous referee for many insightful comments, which significantly improved the paper. We are indebted to M. Malkan for many valuable comments and suggestions. We thank D. Sanders and J. M. Mazzarella for useful discussions.

TG acknowledges financial support from the Japan Society for the Promotion of Science (JSPS) through JSPS Research Fellowships for Young Scientists.

This research is based on the observations with *AKARI*, a JAXA project with the participation of ESA.

The authors wish to recognize and acknowledge the very significant cultural role and reverence that the summit of Mauna Kea has always had within the indigenous Hawaiian community. We are most fortunate to have the opportunity to conduct observations from this sacred mountain.

Support for the work of ET was provided by the National Aeronautics and Space Administration through Chandra Postdoctoral Fellowship Award Number PF8-90055 issued by the Chandra X-ray Observatory Center, which is operated by the Smithsonian Astrophysical Observatory for and on behalf of the National Aeronautics and Space Administration under contract NAS8-03060.

TTT has been supported by the Program for Improvement of Research Environment for Young Researchers from Special Coordination Funds for Promoting Science and Technology, and the Grant-in-Aid for the Scientific Research Fund (20740105) commissioned by the Ministry of Education, Culture, Sports, Science and Technology (MEXT) of Japan. TTT has been also partially supported from the Grand-in-Aid for the Global COE Program 'Quest for Fundamental Principles in the Universe: from Particles to the Solar System and the Cosmos' from the MEXT.

REFERENCES

Aird J. et al., 2010, MNRAS, 401, 2531
Babbedge T. S. R. et al., 2006, MNRAS, 370, 1159
Barger A. J. et al., 2005, AJ, 129, 578
Bavouzet N., Dole H., Le Floc'h E., Caputi K. I., Lagache G., Kochanek C. S., 2008, A&A, 479, 83
Boquien M. et al., 2010, ApJ, 713, 626
Caputi K. I. et al., 2007, ApJ, 660, 97
Chary R., Elbaz D., 2001, ApJ, 556, 562 (CHEL)
Croom S. M., Smith R. J., Boyle B. J., Shanks T., Miller L., Outram P. J., Loaring N. S., 2004, MNRAS, 349, 1397
Dale D. A., Helou G., 2002, ApJ, 576, 159
Dunne L., Eales S. A., 2001, MNRAS, 327, 697
Gandhi P. et al., 2009, A&A, 502, 457
Goto T., 2005, MNRAS, 360, 322
Goto T., 2006, MNRAS, 369, 1765
Goto T. et al., 2010, A&A, 514, A6
Gruppioni C. et al., 2010, A&A, 518, L27
Hasinger G., Miyaji T., Schmidt M., 2005, A&A, 441, 417
Ishihara D. et al., 2010, A&A, 514A, 1
Jeong W.-S. et al., 2007, PASJ, 59, 429
Kartaltepe J. S. et al., 2010, ApJ, 709, 572
Kennicutt R. C., Jr, 1998, ARA&A, 36, 189
Kewley L. J., Groves B., Kauffmann G., Heckman T., 2006, MNRAS, 372, 961
Lagache G., Dole H., Puget J.-L., 2003, MNRAS, 338, 555
Le Floc'h E. et al., 2005, ApJ, 632, 169
Magnelli B., Elbaz D., Chary R. R., Dickinson M., Le Borgne D., Frayer D. T., Willmer C. N. A., 2009, A&A, 496, 57
Mould J. R. et al., 2000, ApJ, 529, 786
Murakami H. et al., 2007, PASJ, 59, 369
Pérault M., 1987, PhD thesis, Université Paris VII
Pérez-González P. G. et al., 2005, ApJ, 630, 82
Pozzi F. et al., 2004, ApJ, 609, 122
Richards G. T. et al., 2006, AJ, 131, 2766
Rodighiero G. et al., 2010, A&A, 515, A8
Rush B., Malkan M., Spinoglio L., 1993, ApJS, 89, 1
Sanders D. B., Mazzarella J. M., Kim D.-C., Surace J. A., Soifer B. T., 2003, AJ, 126, 1607
Saunders W. et al., 1990, MNRAS, 242, 318
Schiminovich D. et al., 2005, ApJ, 619, L47
Schmidt M., 1968, ApJ, 151, 393
Sedgwick C. et al., 2010, MNRAS, submitted
Siebenmorgen R., Krügel E., 2007, A&A, 461, 445
Spinoglio L., Malkan Rush B., Carrasco L., Recillas-Cruz E., 1995, ApJ, 435, 616
Smith J. D. T. et al., 2007, ApJ, 656, 770
Symeonidis M., Page M. J., Seymour N., Dwelly T., Coppin K., McHardy I., Rieke G. H., Huynh M., 2009, MNRAS, 397, 1728
Takeuchi T. T., Yoshikawa K., Ishii T. T., 2000, ApJS, 129, 1
Takeuchi T. T., Yoshikawa K., Ishii T. T., 2003, ApJ, 587, L89
Takeuchi T. T., Buat V., Iglesias-Páramo J., Boselli A., Burgarella D., 2005, A&A, 432, 423
Takeuchi T. T., Ishii T. T., Dole H., Dennefeld M., Lagache G., Puget J.-L., 2006, A&A, 448, 525
Treister E., Urry C. M., Virani S., 2009, ApJ, 696, 110
Treister E. et al., 2010, Sci, in press
Ueda Y., Akiyama M., Ohta K., Miyaji T., 2003, ApJ, 598, 886
Wright E. L., 2008, in Zinnecker H., Epchtein N., Rauer H., eds, EAS Publ. Ser. Vol. 33, The Astrophysical Science Cases at Dome C. European Astronomical Society, Versoix, Switzerland, p. 57
Yamamura I. et al., 2009, in Usuda T, Tamura M., Ishii M., eds, AIP Conf. Proc. Vol. 1158, Exoplanets and Disks: Their Formation and Diversity. Am. Inst. Phys., Melville, NY, p. 169
Yuan T.-T., Kewley L. J., Sanders D. B., 2010, ApJ, 709, 884

This paper has been typeset from a TEX/LATEX file prepared by the author.